Applied Catalysis B: Environmental 97 (2010) 204–212

Contents lists available at ScienceDirect

Applied Catalysis B: Environmental

journal homepage: www.elsevier.com/locate/apcatb

Study on the co-catalytic effect of titanate nanotubes on Pt-based catalysts in direct alcohol fuel cells

Pu Xiao[a,b], Huanqiao Song[a], Xinping Qiu[a,b,*], Wentao Zhu[a], Liquan Chen[a,b], Ulrich Stimming[c], Petra Bele[c]

[a] Key Laboratory of Organic Optoelectronics and Molecular Engineering, Department of Chemistry, Tsinghua University, Beijing 100084, China
[b] Laboratory of Advanced Power Sources, Graduate School at Shenzhen, Tsinghua University, Shenzhen 518055, China
[c] Department of Physics E19, Technical University of Munich, Garching D-85748, Germany

ARTICLE INFO

Article history:
Received 16 December 2009
Received in revised form 22 March 2010
Accepted 6 April 2010
Available online 10 April 2010

Keywords:
TiO_2
Titanate nanotube
Direct ethanol fuel cell
Anode catalyst
Co-catalytic effect

ABSTRACT

In this paper, titanate nanotubes were synthesized and their co-catalytic effects in direct alcohol fuel cells (DAFC) were studied by physically mixing them with commercial Pt/C catalyst. BET results showed the surface area increased significantly when a big amount of nanotubes were formed. Infrared (IR) spectra and thermal gravity analysis (TGA) showed that less water existed in nanoparticles and nanotubes when the raw materials were calcinated at higher temperature. Electrochemical measurements showed that titanate nanotubes which contained more structural water had a better catalytic performance. Proton conductivity of titanate nanotubes was also considered to be an important factor for enhancing oxidation reactivity and was studied by impedance tests.

1. Introduction

In recent years, direct alcohol fuel cells (DAFC) have attracted more and more attentions due to their potential application in portable electronic devices and electric vehicles [1,2]. However, the use of Pt-based catalysts which are easily poisoned by intermediate impedes a widespread commercialization of DAFC [3–5]. In order to solve this problem, some metals (Ru, Sn, Os, Mo, W, etc.) [6–9] and metal oxides (RuO_2, ZrO_2, CeO_2, TiO_2, SnO_2, etc.) [10–15] are added into Pt-based catalyst to enhance the CO tolerance based on the bi-functional mechanism and the electronic effect [4].

Recently, TiO_2 has been used in fuel cell due to its co-catalytic activity, stability in both acid and basic, non-toxicity and relatively low cost. By using TiO_2 or composited TiO_2 nanomaterials as catalyst support [14,16–25] or co-catalysts [26–29] for DAFC, the performance of catalyst was improved [30]. TiO_2 nanomaterials could increase the oxidation current of fuel cell by introducing UV light to the fuel cell system due to its photocatalytic properties [31–33]. Among the different nanostructures of TiO_2, TiO_2 nanotubes which were discovered by Kasuga et al. [34] in 1998, have shown high activity as co-catalysts and catalyst supports in anode catalysts for DAFC [16,19,29,35]. The TiO_2 nanotubes are usually synthesized via the reaction of TiO_2 particles with NaOH aqueous solution [36–40]. Using different raw materials and hydrothermal synthetic conditions, the nanostructures of nanotubes would be different [41]. This tubular structure has larger surface area and certain degree of porosity, thus showed good activity and is good for mass transmission.

However, the crystal phases of TiO_2 nanotubes used for DAFC were all described as anatase or a mixture of anatase and rutile in former works, TiO_2 nanotubes with titanate crystal phase used for DAFC anode catalysts has not been reported yet. Titanate crystal structure is a newly discovered structure. It is believed to be constructed from layered trititanate $H_2Ti_3O_7$, and protons exist between the layers [36]. This material may have good proton conductivity and could be used as DAFC co-catalysts or proton exchange membrane additive. Also, further study on the co-catalytic effect of TiO_2 is necessary to be done.

In this paper, titanate nanotubes were synthesized and mixed with commercial Pt/C catalyst to promote alcohol oxidation. The electrochemical measurements and material analyses were carried out to study the co-catalytic effect of titanate nanotubes. In addition, the comparison was made between different TiO_2 nanoparticles and titanate nanotubes.

* Corresponding author at: Key Laboratory of Organic Optoelectronics and Molecular Engineering, Department of Chemistry, Tsinghua University, Beijing 100084, China. Tel.: +86 10 62794234; fax: +86 10 62794234.
E-mail address: qiuxp@mail.tsinghua.edu.cn (X. Qiu).

0926-3373/$ – see front matter © 2010 Elsevier B.V. All rights reserved.
doi:10.1016/j.apcatb.2010.04.001

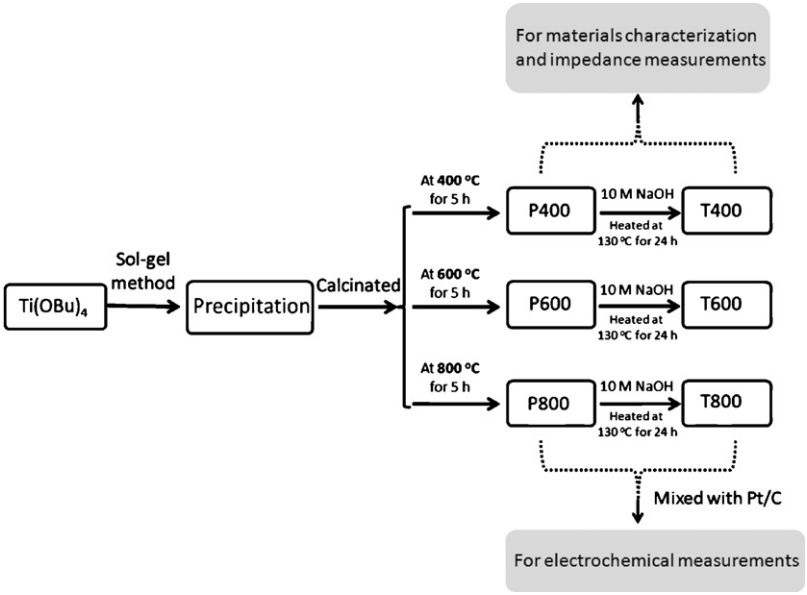

Fig. 1. Flow chart of the synthesis steps and testing procedures.

2. Experimental

2.1. Preparation of titanate nanotubes

The brief flow chart of the synthesis steps and following measurements is shown in Fig. 1. The TiO_2 nanoparticles were first prepared using sol–gel method as described in Ref. [42]. A solution contained 10 ml $Ti(OBu)_4$ and 100 ml ethanol was drop-wise introduced into a solution of 30 ml water and 100 ml glacial acetic acid at a rate of 3 ml/min. After aging for 12 h at room temperature, this powder was dried at 80 °C. The precursor was put into a muffle oven and heated at 400, 600 and 800 °C for 5 h. In this way we received particles named as: P400, P600 and P800. Then, 0.5 g of the obtained TiO_2 nanoparticles were mixed with 30 ml 10 M NaOH aqueous solution and stirred for 30 min. The mixture was placed into a Teflon-lined autoclave and heated at 130 °C for 24 h. The precipitate was washed with 0.1 M HNO_3 aqueous solution and deionized water until pH < 7; afterwards they were separated by centrifugation and dried at 80 °C. The titanate nanotubes we got were named as: T400, T600 and T800 using P400, P600 and P800 as raw material.

2.2. Characterization of TiO_2 nanomaterials

The morphology of the TiO_2 nanomaterials was observed on a JEOL model JEM-1200EX transmission electron micrograph (TEM). The EDX analysis was carried out at 150 kV using an OXFORD INCA 300 energy dispersive X-ray spectrometer attached to a scanning electron microscope. The X-ray diffraction (XRD) spectra were collected on a Bruker D8 advanced diffractometer using Cu Kα as the radiation source. The TGA was carried out using Universal V5.3C 2050 Instrument in the temperature range of room temperature to 900 °C with a scanning rate of 10 °C min^{-1}. The surface areas of TiO_2 nanotubes and titanate nanotubes were measured by BET measurements. A PE (Spectrum One) spectrometer was used for the IR measurements. In order to measure the conductivity, the nanotube powder was pressed into a pellet (14 mm in diameter) using an axial pressure of ca. 9 t. Then a thin layer of gold was painted on both sides of the pellet. Alternating current (ac) impedance was carried out at room temperature using a PARSTAT 2273 workstation over a frequency range of 10^{-1} to 2×10^6 Hz. Electronic resistance was measured by applying a dc voltage scan from −0.1 V to 0.1 V and recorded the current response.

2.3. Electrochemical measurement

The catalyst slurry was prepared by physically mixing Pt/C (E-TEK, 10 wt% Pt on Vulcan) catalyst with TiO_2 nanoparticles and titanate nanotubes as described in Ref. [30], then 20 μL slurry was casted on glassy carbon (7 mm in diameter) and air-dried at 80 °C for 45 min. The weight ratio of titanate nanotubes (or TiO_2 nanoparticles): Pt/C = 1:5. Electrochemical measurements were carried out in a three electrode cell using an Autolab PGSTAT 20 at 25 °C. A glassy carbon coated with catalyst ink was used as working electrode. An Hg/Hg_2SO_4 electrode (0.5 M H_2SO_4) and Pt foil were used as reference and counter electrodes, respectively. All electrode potentials were measured against the Hg/Hg_2SO_4 electrode (0.5 M H_2SO_4) and later converted to against a normal hydrogen electrode (NHE). A solution of 1 M $HClO_4$ or 1 M CH_3OH + 1 M $HClO_4$ or 1 M C_2H_5OH + 1 M $HClO_4$ was used as electrolyte. The potential range of cyclic voltammogram was from 0.04 to 1.24 V vs. NHE at a scan rate of 50 mV s^{-1}. The oxidation of pre-adsorbed CO was measured by CO stripping voltammetry in 1 M $HClO_4$ solution at a scan rate of 10 mV s^{-1}. Chronoamperometric curves of CO ad-layer oxidation, methanol oxidation and ethanol oxidation were recorded in 1 M $HClO_4$ at 0.74 V (vs. NHE), 1 M CH_3OH + 1 M $HClO_4$ at 0.84 V (vs. NHE) and 1 M C_2H_5OH + 1 M $HClO_4$ at 0.78 V (vs. NHE), respectively. The voltage value for chronoamperometric measurements is determined by observing the cyclic voltammetry curves. The proper potential is at which the oxidation current increases rapidly.

Table 1
Particle sizes and crystal phases of TiO_2 nanoparticles and titanate nanotubes.

Sample	Calcination temperature (°C)	Crystal phase	Particle size (nm)	
			XRD	TEM
P400	400	Anatase	12	11.5
P600	600	Anatase	35	34.6
P800	800	Rutile and anatase	71	99.9
T400	–	Titanate	–	–
T600	–	Titanate and anatase	–	–
T800	–	Titanate, anatase and rutile	–	–

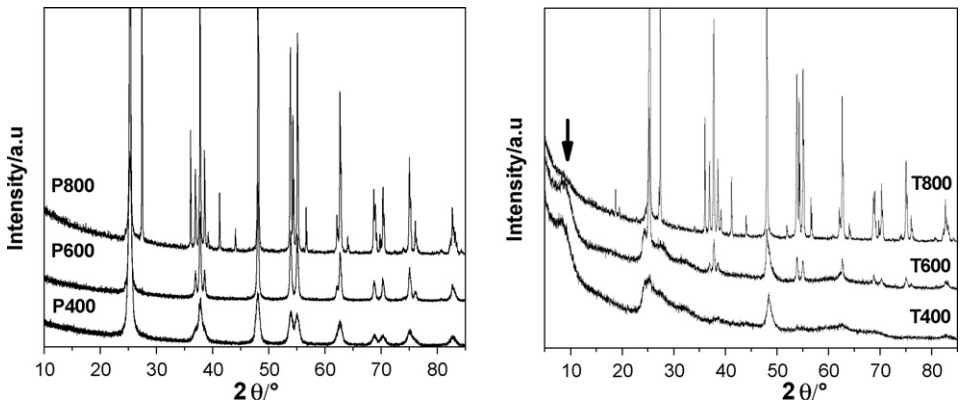

Fig. 2. XRD patterns of (a) TiO_2 nanoparticles and (b) titanate nanotubes.

3. Results and discussion

3.1. The structure characterization of synthesized TiO_2 nanoparticles and titanate nanotubes

According to the different calcination temperatures, TiO_2 nanoparticles are named as P400, P600 and P800. Following the nomenclature of the different TiO_2 nanoparticles which are used as raw materials for reaching the titanate nanotubes, the titanate nanotubes are named as T400, T600 and T800. From Table 1 we could find that the particle size increases with calcination temperature because of agglomeration. Anatase phase is formed while samples being heated below 800 °C, and 47 wt% rutile phase formed when calcination temperature reaches 800 °C. There are several parameters such as crystallinity, surface area and density of surface hydroxy groups would affect the activity of TiO_2, and crystal form is believed to be the most important factor [43–45]. Though rutile phase is believed to have lower catalytic activity in photo-

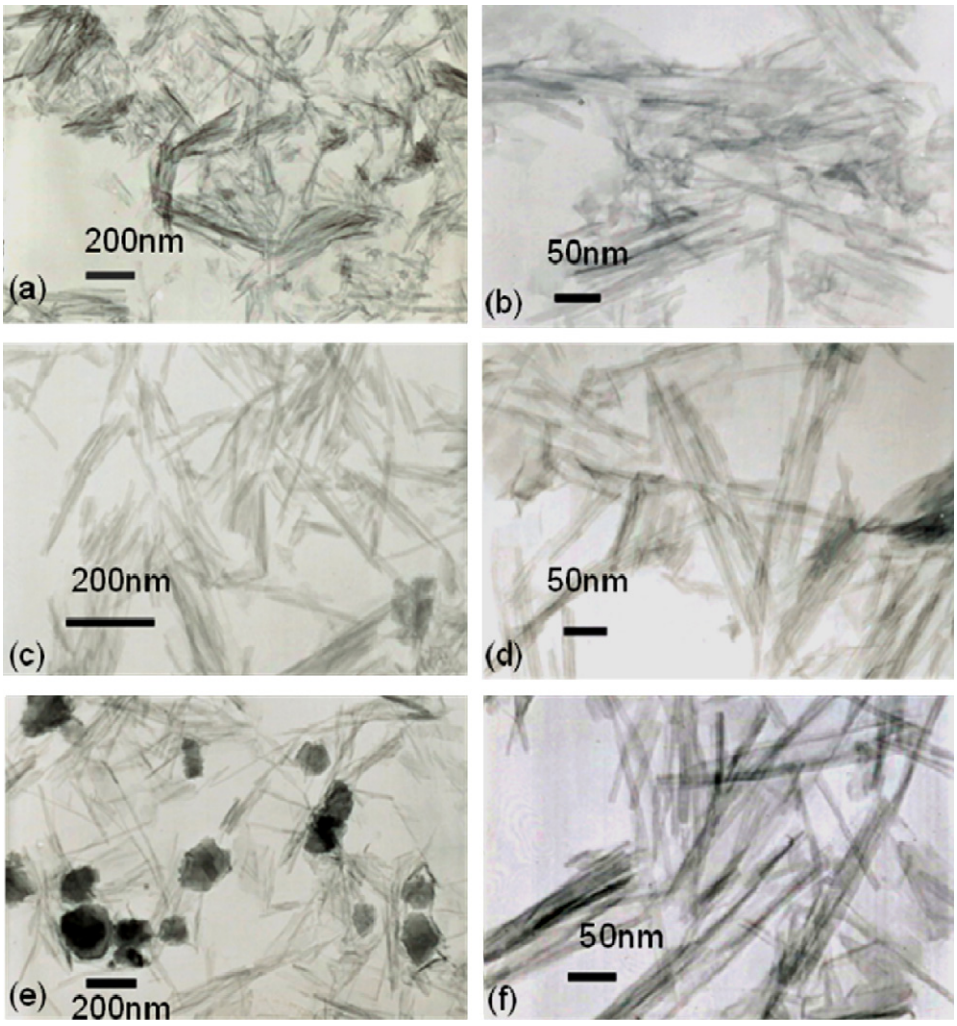

Fig. 3. TEM images of titanate nanotubes. (a and b) T400, (c and d) T600, (e and f) T800.

Table 2
BET surface areas of TiO_2 nanoparticles and titanate nanotubes.

Sample	Specific surface areas (m^2/g)
P400	118.64
P600	21.54
P800	0.83
T400	254.95
T600	199.52
T800	10.75

catalysis [46], a mixture of rutile and anatase like P25 has higher activity than pure anatase due to the high charge separation efficiency. So P800 might have a higher activity than P400 and P600 after mixing with Pt/C.

The formation steps of titanate nanotubes are: (1) dissolution of TiO_2 nanoparticles in NaOH aqueous solution to form nanosheets of sodium titanate, (2) wrapping of nanosheets into tubular structure, (3) exchange of sodium ions by proton during acid washing procedure [36,39]. The dimensions of the nanotubes are relatively independent of the particle size of TiO_2 crystals [47], but there will be a low product yield of nanotubes if the TiO_2 nanoparticles could not be fully solved under certain hydrothermal condition. P400 and P600 are typical anatase while P800 is a mixture of anatase and rutile in Fig. 2(a), and the peaks become sharper with increasing calcinating temperature which indicates a growth in the particle size. As shown in Fig. 2(b), the peak appears around $2\theta = 10^\circ$ is the typical peak of layered titanate structure [40]. Since T400 and T600 mainly present titanate phase, they should have a high production rate of nanotubes. The XRD pattern of T800 is very similar to that of P800, which indicates that a large amount of nanoparticles still exist in T800.

Fig. 3 shows the TEM images of titanate nanotubes synthesized from different TiO_2 nanoparticles. The diameters of the nanotubes are about 10 nm, and the lengths of the tubes have a range from several tens to several hundreds of nanometers. A big amount of nanoparticles appear in the TEM images of T800, which confirms a low rate of the conversion from nanoparticles to nanotubes. BET measurements shown in Table 2 were carried out to study the surface area of samples and provide more information for the nanotubes generation rate. The surface area of nanoparticles decreases rapidly with increasing calcination temperature due to the increasing particle size. Too small surface area would cause a bad contact between TiO_2 and Pt/C catalyst, so the co-catalytic effect would be relatively weak for P600 and P800. The very small surface area of T800 also confirms that much fewer nanotubes are formed using P800 as raw material. Combined with the XRD results we could find that P800 has a low yield to form nanotubes because the activity of rutile phase is lower than that of anatase and the formation of nanosheet from too large particles would be slow. Due to the big surface area of T400 and T600, the contact between titanate nanotubes and Pt/C would be better than that of other samples which may result in a remarkable co-catalytic effect.

The water and OH group contained in oxide play an important role in oxidizing CO-like species according to bi-functional mechanism, so IR and thermal analysis were carried out to study the content of water in our samples. As shown in Fig. 4, the IR peaks around 1630 and 3400 cm^{-1} attribute to a bending vibration of H–O–H and a stretching vibration of O–H, respectively [36]. By comparing the IR spectra, it can be seen that T400 and T600 contain much more structure water and OH group than other samples. Since IR could only be used for qualitative analysis, TGA data are used for quantitative analysis of water content in particles and nanotubes as shown in Fig. 5. EDX results show the amount of Na^+ is below 0.5 wt% in nanotubes, so the titanate nanotubes are considered to be only composed of Ti, O and H elements. Assuming that the weight decrease between room temperature and 100 °C is attributed to

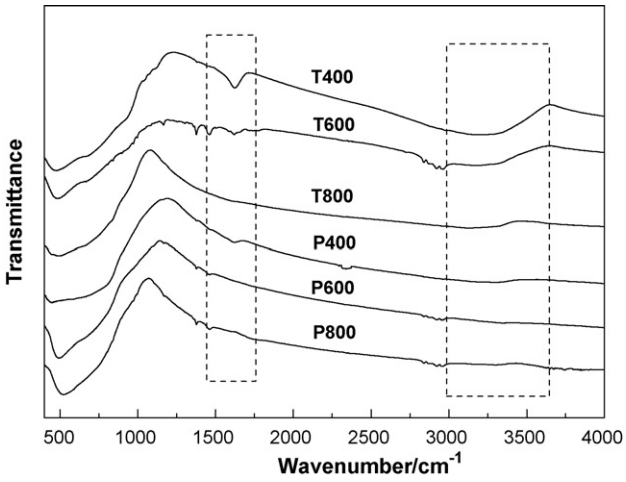

Fig. 4. IR spectra of TiO_2 nanoparticles and titanate nanotubes.

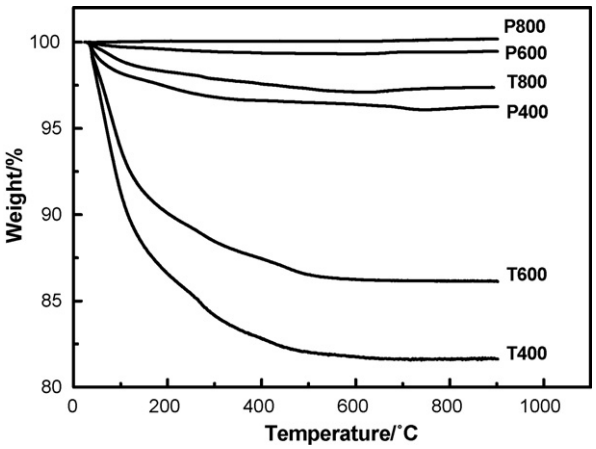

Fig. 5. TGA results of TiO_2 nanoparticles and titanate nanotubes.

the loss of adsorbed water and the weight decrease above 100 °C is attributed to the loss of structural water [47], the water contents of samples are calculated and listed in Table 3. T400 and T600 contain much more adsorbed and structural water than other samples, and T400 has the largest amount of water. Since the structural water in TiO_2 could enhance the oxidation of CO species [35], it can be inferred that T400 and T600 should have much better co-catalytic activity than other samples.

3.2. Conductivity studies on titanate nanotubes

For methanol oxidation, the anode reaction is shown in Eq. (1) [3]:

$$CH_3OH + H_2O \rightarrow CO_2 + 6H^+ + 6e^- \quad (1)$$

Table 3
Water contents of TiO_2 nanoparticles and titanate nanotubes.

Sample	Weight loss (wt%)	H_2O content per TiO_2 formula unit (mol)		
		Total	Adsorbed H_2O	Structure H_2O
P400	3.74	0.17	0.08	0.09
P600	0.54	0.02	0.02	0.01
P800	0	0	0	0
T400	18.37	1.00	0.48	0.52
T600	13.88	0.72	0.32	0.39
T800	2.62	0.12	0.05	0.07

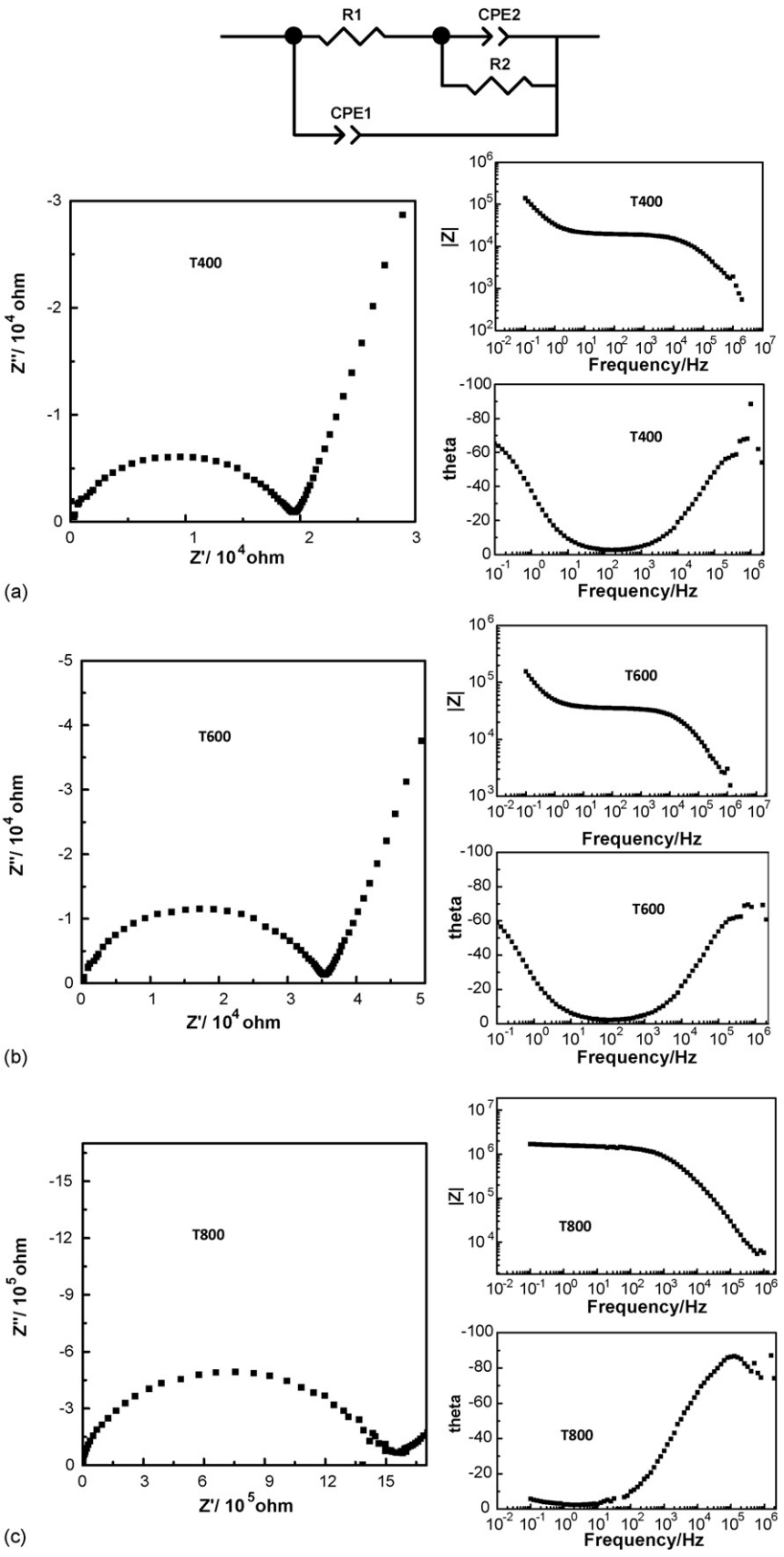

Fig. 6. Impedance plane and equivalent circuit of T400, T600 and T800.

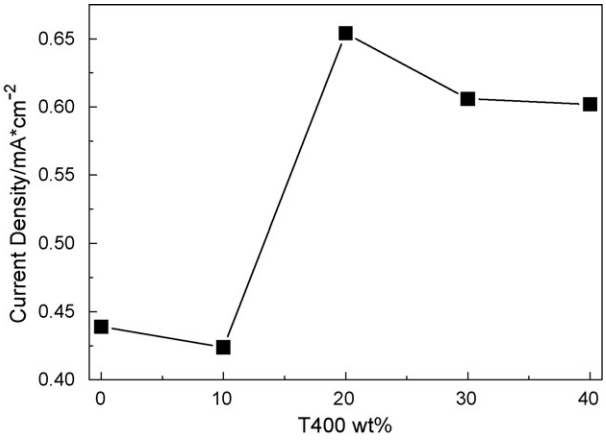

Fig. 7. Methanol oxidation current of Pt/C with different amount of T400 in 1 M CH_3OH + 1 M $HClO_4$ in the potential range 0.04–1.24 V vs. NHE at a scan rate of 50 mV s^{-1} at 25 °C.

For ethanol oxidation, the anode reaction is shown in Eq. (2) [48]:

$$C_2H_5OH + 3H_2O \rightarrow 2CO_2 + 12H^+ + 12e^- \quad (2)$$

Because protons are produced during alcohol oxidation process, alcohol oxidation could be enhanced by removing the protons from reaction sites. So the proton conductivity of catalyst is believed to be as important as electron conductivity [11]. Titanate nanotubes synthesized by hydrothermal method are believed to be constructed from layered trititanate $H_2Ti_3O_7$, and protons exist between the layers [36]. Since cations could transfer along the length of the nanotube [49], titanate nanotubes should have good proton conductivity.

Conductivity studies were carried out to compare the protonic conductions of different titanate nanotube samples. The impedance spectra and equivalent circuit of T400, T600 and T800 are shown in Fig. 6. Both protonic and electronic resistances make contribution to R_1. CPE_1 is the geometric capacitance and CPE_2 is the double layer capacitance. R_2 represents the resistance of the blocking electrodes. Since the value of R_1 obtained from the impedance spectra includes both the proton resistance and electron resistance, proton conductivity was calculated by taking out electron resistance and normalized by the thickness and size of pallet. From Table 4 we could see that the value order of proton conductivity is T400 > T600 ≫ T800. The electronic conductivity values of nanotubes are much smaller than proton conductivity values, so the total conductivity mainly attributes to proton conductivity. The proton conductivity and geometric capacitance value of T800 is much smaller than that of T400 and T600 because of a low production yield of nanotubes. And higher proton conductivity should result in a more active catalyst as described in literature [11,50,51].

3.3. Electrochemical properties and studies

The optimized ratio of Pt/C and titanate nanotube is obtained by mixing Pt/C with different amount of T400 and their methanol oxidation current densities are shown in Fig. 7. Pt/C mixed with 20 wt% titanate nanotube is considered to be an optimized ratio for further investigation.

Fig. 8 shows the CV curves of alcohol electro-oxidation at Pt/C and Pt/C +20 wt% TiO_2 nanomaterials. The alcohol oxidation current of Pt/C catalysts remarkably increases after mixing with T400 and T600, and almost remains the same after mixing with T800. This result shows good consistency with conductivity result. But TiO_2 nanoparticles do not enhance the oxidation reactivity while another report [29] shows that TiO_2 nanoparticles could also slightly enhance the oxidation reactivity of Pt/C. There are two possible explanations for this phenomenon: (i) as reported in the literature, the peak current density increases due to the increase of electrochemical active surface (EAS). However, if the peak current density is normalized with EAS, the catalytic activity of Pt/C added with TiO_2 nanoparticles also decreases. In Xi's [30] model, the oxide could enhance the utilization of Pt by diluting effect. And the Pt/C (10 wt.% Pt on Vulcan) catalyst we used here has a low Pt loading and a good dispersion which causes a much higher utilization of Pt compared to Pt/C (20 wt.% Pt on Vulcan) catalyst used in Ref. [29]. Thus the oxide could hardly increase the catalytic activity by increasing EAS, and the existing nanoparticles somehow are not good for mass transmission causing a decrease in oxidation reactivity. On the other hand, it could be indicated that the diluting effect would be more remarkable while the Pt loading is higher. (ii) The ratios of Pt/C to TiO_2 nanoparticles are different in our experiments and in literature [29]. As shown in Fig. 7, small amounts of TiO_2 will not enhance the catalytic activity because of bad contact of nanoparticles, and large amounts of TiO_2 will decrease the catalytic activity because of the low electron conductivity of oxide. In our experiments, the optimized amount of TiO_2 nanotubes to mix with Pt/C was chosen, and the same amount of TiO_2 nanoparticles was added to Pt/C for comparison, so it might not be also an optimized ratio for TiO_2 nanoparticles. It is worth noting that although the catalytic activity of Pt/C all decreased after mixing with nanoparticles, Pt/C + P800 has relatively higher catalytic activity than Pt/C + P400 and Pt/C + P600. That is because the particle size of P800 is too big to get a good dispersion in Pt/C, so the mass transmission blocking effect is low. But particles of P800 still block some of the mass transfer channels so the alcohol oxidation current of Pt/C + P800 is lower than that of Pt/C.

According to bi-function mechanism, the OH species absorbed on the surface of oxide could accelerate the electro-oxidation of adsorbed intermediate on the electrode, so the nanomaterial with bigger amount of structure water would have higher co-catalytic effect. From TGA result we could find that the co-catalytic effect of nanotubes shows good consistency with the amount of structure water. As shown in Fig. 8(a–c), the backward methanol oxidation peaks increase more significantly than the forward scan peaks after Pt/C mixing with nanotubes. Literature [52,53] has reported the backward scan peak is related to the oxidation of intermediate species on the surface, so titanate nanotubes containing considerable oxygen-containing species would accelerate the oxidation of intermediate species and reach higher current density. For ethanol oxidation as shown in Fig. 8(d–f), the backward scan peaks have a consistent change with the forward scan peeks. Because the intermediate species of ethanol such as Pt–OCH_2CH_3, Pt–CHOH–CH_3, $(Pt)_2$ COH–CH_3 and Pt–$COCH_3$ [54] all contain C–C bonds, and the break of C–C bonds could not be accelerated by introducing more oxygen-containing species. However, by comparing the water content in nanoparticles and nanotubes, for example, T800 and P400, we could see that more water is in P400 than in T800, but T800 has higher co-catalytic effect than P400. This may because nanotubes with hollow structure are good for mass transmission, but nanoparticles with different particle sizes would cause different dispersion states in Pt/C catalyst and block the mass transmission, which seemed to be more important than the water content factor. So the oxidation reactivity of Pt/C decreases after mixed with TiO_2 nanoparticles.

For both methanol and ethanol oxidation, $(CO)_{ads}$ will cause Pt catalyst poisoning [3,48]. Some metals and oxides containing OH species could oxidize $(CO)_{ads}$ and release Pt active sites. In order to investigate the co-catalytic effect of TiO_2 nanotubes, CO stripping and chronoamperometry were carried out

Table 4
Impedance data of different titanate nanotube samples (inclusive of sample geometry correction).

Sample	Electronic conductivity ($S\,cm^{-1}$)	Proton conductivity ($S\,cm^{-1}$)	Geometric capacitance value ($F\,cm^{-1}$)
T400	6.02×10^{-8}	3.38×10^{-6}	2.59×10^{-10}
T600	9.33×10^{-8}	2.30×10^{-6}	1.64×10^{-10}
T800	6.20×10^{-8}	1.07×10^{-7}	3.74×10^{-11}

to study CO oxidation behavior as shown in Fig. 9. From the CO stripping curves it could be seen that the CO oxidation starting potential and peak potential all become lower after mixing with nanotubes. CO ad-layer electro-oxidation curves shows the time order of CO electro-oxidation peaks appeared is Pt/C + T400 < Pt/C + T600 < Pt/C + T800 ≈ Pt/C, which proofs the structure water in nanotubes could accelerate the electro-oxidation of CO_{ads} through a bi-functional approach. Furthermore, for ethanol oxidation, not only CO oxidation but also C–C bond scission is important [55]. Other measurements such as differential electrochemical mass spectrometry (DEMS) would be helpful for further study [55,56]. Since the catalyst slurry volume painted on glassy carbon is fixed, less Pt/C exited on working electrode because nanotubes take some volume. So the electrochemical active surface area (EAS) of Pt decreases after being mixed with nanotubes.

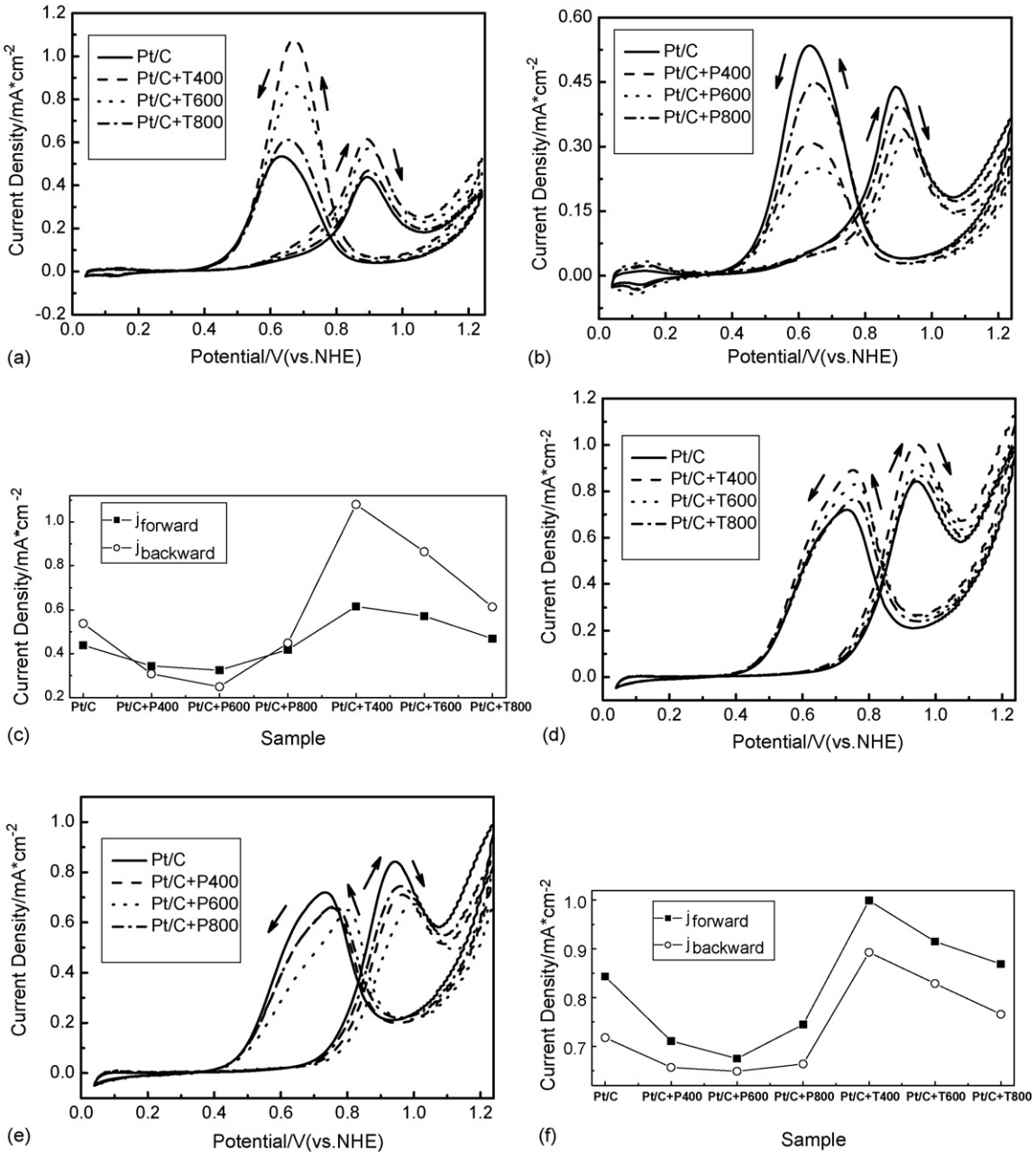

Fig. 8. CVs of alcohol electro-oxidation at (a) Pt/C and Pt/C + 20 wt% TiO_2 nanotubes, (b) Pt/C and Pt/C + 20 wt% TiO_2 nanoparticles in 1 M CH_3OH + 1 M $HClO_4$, (c) compare of methanol oxidation peak current density, (d) Pt/C and Pt/C + 20 wt% TiO_2 nanotubes, (e) Pt/C and Pt/C + 20 wt% TiO_2 nanoparticles in 1 M C_2H_5OH + 1 M $HClO_4$ in the potential range 0.04–1.24 V vs. NHE at a scan rate of 50 mV s^{-1} at 25 °C, (f) compare of ethanol oxidation peak current density.

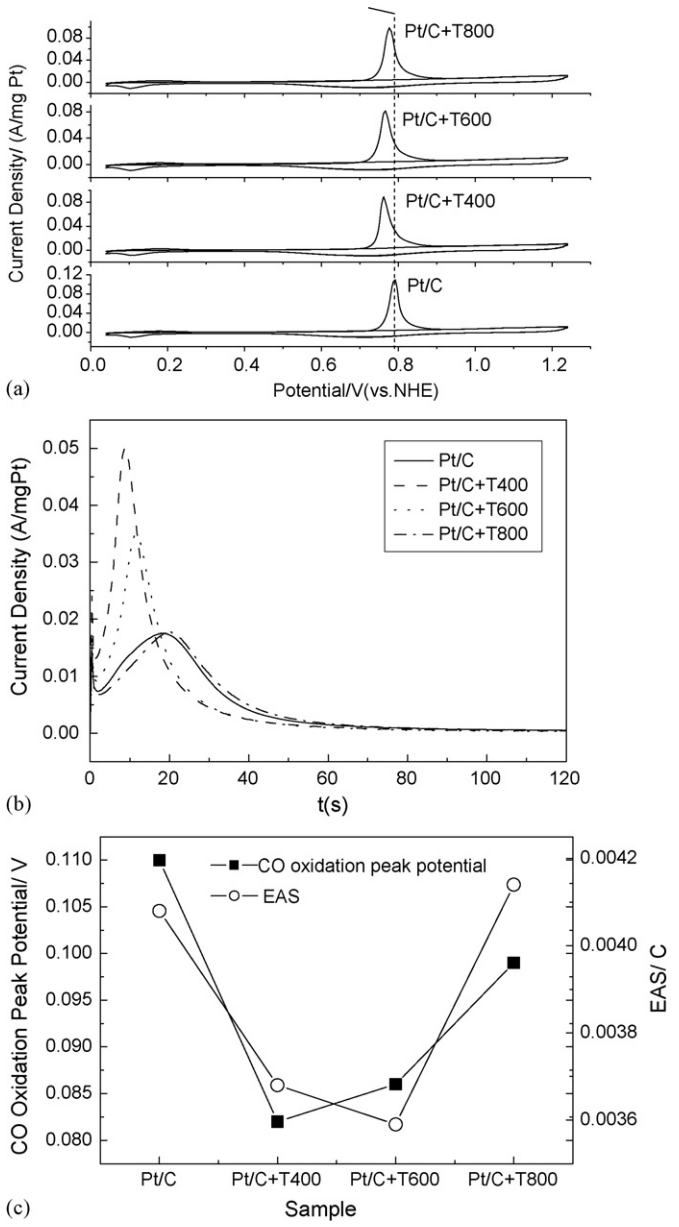

Fig. 9. (a) CO stripping curves and (b) CO ad-layer electro-oxidation curves for Pt/C and Pt/C + 20 wt% TiO_2 nanotubes in 1 M $HClO_4$, (c) compare of CO oxidation peak potential and compare of EAS values.

To study the co-catalytic effect of nanotubes, chronoamperometry measurements were also carried out in alcohol solution as shown in Fig. 10. The pretreatment of working electrode was carried out as described in Ref. [35]. In Fig. 10(a) we could see that the current densities decrease with time, and Pt/C + T400 which contains the most structure water shows the highest current density during the testing period. Pt/C + T600 has less structure water than Pt/C + T400, so it has the second highest current density. Since Pt/C + T800 contains little structure water and the existence of big size nanoparticles would block the mass transmission, its current density is even lower than that of Pt/C catalyst. In Fig. 10(b), the current densities on Pt/C + T400 and Pt/C + T600 have similar values and are both higher than that on Pt/C. The current density on Pt/C + T800 becomes much lower than that on Pt/C, because ethanol molecule is bigger than methanol molecule; thereby the mass transmission blocking effect becomes more serious.

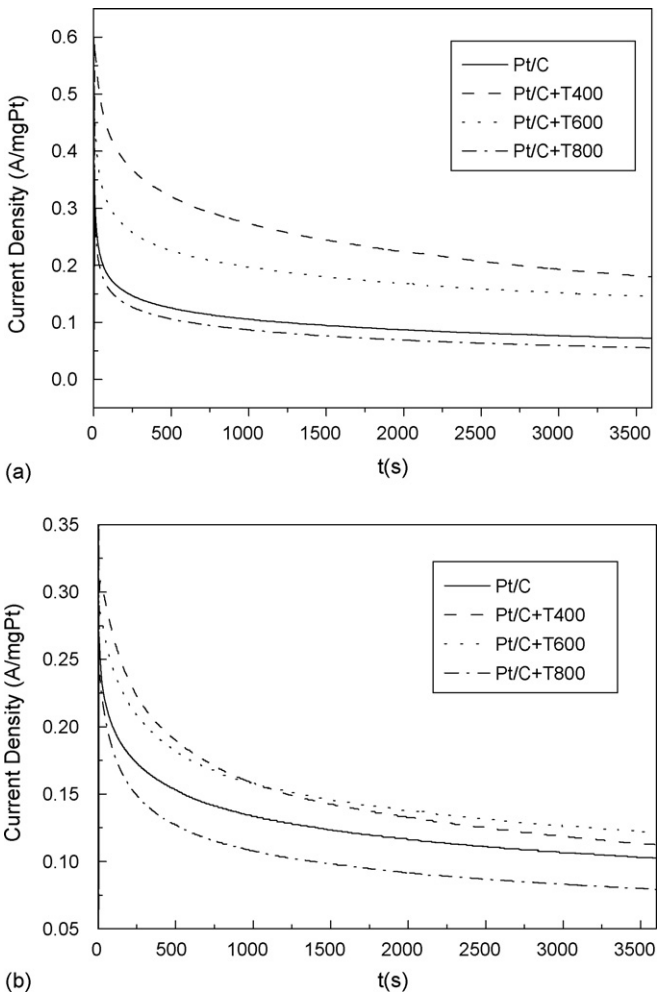

Fig. 10. Current density–time curves at Pt/C and Pt/C + 20 wt% TiO_2 nanomaterials (a) at 0.84 V (vs. NHE) in 1 M CH_3OH + 1 M $HClO_4$, (b) at 0.78 V (vs. NHE) in 1 M C_2H_5OH + 1 M $HClO_4$.

4. Conclusions

Different titanate nanotubes were synthesized and their co-catalytic effect was studied by structure characterization and electrochemical measurements. The product yield of nanotubes is related to the raw material. Anatase TiO_2 nanoparticles with small particle size has higher rate to produce nanotubes. Titanate nanotubes could accelerate the alcohol oxidation while TiO_2 nanoparticles showed no improvement. The catalytic activity order of catalysts is Pt/C + T400 > Pt/C + T600 (Pt/C + T800. Pt/C + T400 has the best alcohol oxidation activity and CO stripping tests showed it has the lowest oxidation potential. Combining with material analysis and conductivity tests, we found three factors that affect the co-catalytic activity of titanate nanotubes: (i) more structure water in nanotubes could accelerate the oxidation of CO_{ads} through a bi-functional approach. (ii) Tube-like structure is good for the mass transmission. (iii) High proton conductivity will result in a higher catalytic activity. TiO_2 nanoparticles were used for comparison and the diluting effect was found that may enhance the oxidation reactivity of Pt/C catalyst while mass transmission blocking may cause a decrease in the catalyst activity.

Acknowledgements

The authors appreciate the financial support of the State Key Basic Research Program of PRC (2009CB220105), National Natu-

ral Science Foundation of China (90410002) and Beijing Natural Science Foundation (2071001).

References

[1] C. Lamy, A. Lima, V. LeRhun, F. Delime, C. Coutanceau, J.M. Leger, J. Power Sources 105 (2002) 283–296.
[2] X.M. Ren, M.S. Wilson, S. Gottesfeld, J. Electrochem. Soc. 143 (1996) L12–L15.
[3] A. Hamnett, Catal. Today 38 (1997) 445–457.
[4] H.A. Gasteiger, N. Markovic, P.N. Ross, E.J. Cairns, J. Phys. Chem. 97 (1993) 12020–12029.
[5] H.A. Gasteiger, N. Markovic, P.N. Ross, E.J. Cairns, J. Electrochem. Soc. 141 (1994) 1795–1803.
[6] B.N. Grgur, G. Zhuang, N.M. Markovic, P.N. Ross, J. Phys. Chem. B 101 (1997) 3910–3913.
[7] K.L. Ley, R.X. Liu, C. Pu, Q.B. Fan, N. Leyarovska, C. Segre, E.S. Smotkin, J. Electrochem. Soc. 144 (1997) 1543–1548.
[8] A.S. Arico, Z. Poltarzewski, H. Kim, A. Morana, N. Giordano, V. Antonucci, J. Power Sources 55 (1995) 159–166.
[9] K.Y. Chan, J. Ding, J.W. Ren, S.A. Cheng, K.Y. Tsang, J. Mater. Chem. 14 (2004) 505–516.
[10] J.S. Wang, J.Y. Xi, Y.X. Bai, Y. Shen, J. Sun, L.Q. Chen, W.T. Zhu, X.P. Qiu, J. Power Sources 164 (2007) 555–560.
[11] L. Cao, F. Scheiba, C. Roth, F. Schweiger, C. Cremers, U. Stimming, H. Fuess, L.Q. Chen, W.T. Zhu, X.P. Qiu, Angew. Chem.-Int. Ed. 45 (2006) 5315–5319.
[12] Y.X. Bai, J.J. Wu, X.P. Qiu, J.Y. Xi, J.S. Wang, J.F. Li, W.T. Zhu, L.Q. Chen, Appl. Catal. B-Environ. 73 (2007) 144–149.
[13] Y.X. Bai, J.J. Wu, J.Y. Xi, J.S. Wang, W.T. Zhu, L.Q. Chen, X.P. Qiu, Electrochem. Commun. 7 (2005) 1087–1090.
[14] H.Q. Song, X.P. Qiu, F.H. Li, Electrochim. Acta 53 (2008) 3708–3713.
[15] L.H. Jiang, G.Q. Sun, Z.H. Zhou, S.G. Sun, Q. Wang, S.Y. Yan, H.Q. Li, J. Tian, J.S. Guo, B. Zhou, Q. Xin, J. Phys. Chem. B 109 (2005) 8774–8778.
[16] Q.Z. Jiang, X. Wu, M. Shen, Z.F. Ma, X.Y. Zhu, Catal. Lett. 124 (2008) 434–438.
[17] S.H. Kang, T.Y. Jeon, H.S. Kim, Y.E. Sung, W.H. Smyrl, J. Electrochem. Soc. 155 (2008) B1058–B1065.
[18] Y. Fu, Z.D. Wei, S.G. Chen, L. Li, Y.C. Feng, Y.Q. Wang, X.L. Ma, M.J. Liao, P.K. Shen, S.P. Jiang, J. Power Sources 189 (2009) 982–987.
[19] M. Wang, D.J. Guo, H.L. Li, J. Solid State Chem. 178 (2005) 1996–2000.
[20] F.P. Hu, F.W. Ding, S.Q. Song, P.K. Shen, J. Power Sources 163 (2006) 415–419.
[21] D. He, L. Yang, S. Kuang, Q. Cai, Electrochem. Commun. 9 (2007) 2467–2472.
[22] E. Formo, Z.M. Peng, E. Lee, X.M. Lu, H. Yang, Y.N. Xia, J. Phys. Chem. C 112 (2008) 9970–9975.
[23] J. Shim, C.R. Lee, H.K. Lee, J.S. Lee, E.J. Cairns, J. Power Sources 102 (2001) 172–177.
[24] L. Xiong, A. Manthiram, Electrochim. Acta 49 (2004) 4163–4170.
[25] P.P. George, V.G. Pol, A. Gedanken, A. Gabashivili, M. Cai, A.M. Mance, L. Feng, M.S. Ruthkosky, J. Fuel Cell Sci. Technol. 5 (2008).
[26] Y.H. Chu, S.W. Ahn, D.Y. Kim, H.J. Kim, Y.G. Shul, H.S. Han, Catal. Today 111 (2006) 176–181.
[27] H.J. Kim, D.Y. Kim, H. Han, Y.G. Shul, J. Power Sources 159 (2006) 484–490.
[28] J.M. Chen, L.S. Sarma, C.H. Chen, M.Y. Cheng, S.C. Shih, G.R. Wang, D.G. Liu, J.F. Lee, M.T. Tang, B.J. Hwang, J. Power Sources 159 (2006) 29–33.
[29] H.Q. Song, X.P. Qiu, X.X. Li, F.S. Li, W.T. Zhu, L.Q. Chen, J. Power Sources 170 (2007) 50–54.
[30] J.Y. Xi, J.S. Wang, L.H. Yu, X.P. Qiu, L.Q. Chen, Chem. Commun. (2007) 1656–1658.
[31] K. Drew, G. Girishkumar, K. Vinodgopal, P.V. Kamat, J. Phys. Chem. B 109 (2005) 11851–11857.
[32] K.W. Park, S.B. Han, J.M. Lee, Electrochem. Commun. 9 (2007) 1578–1581.
[33] D.B. Chu, S.X. Wang, P. Zheng, J. Wang, L.W. Zha, Y.Y. Hou, J.G. He, Y. Xiao, H.S. Lin, Z.W. Tian, ChemSusChem 2 (2009) 171–176.
[34] T. Kasuga, M. Hiramatsu, A. Hoson, T. Sekino, K. Niihara, Langmuir 14 (1998) 3160–3163.
[35] H.Q. Song, X.P. Qiu, D.J. Guo, F.S. Li, J. Power Sources 178 (2008) 97–102.
[36] Q. Chen, G.H. Du, S. Zhang, L.M. Peng, Acta Crystallogr. Sect. B-Struct. Sci. 58 (2002) 587–593.
[37] S. Zhang, L.M. Peng, Q. Chen, G.H. Du, G. Dawson, W.Z. Zhou, Phys. Rev. Lett. 91 (2003) 4.
[38] Z.Y. Yuan, B.L. Su, Colloid Surf. A-Physicochem. Eng. Aspects 241 (2004) 173–183.
[39] D.V. Bavykin, F.C. Walsh, Eur. J. Inorg. Chem. (2009) 977–997.
[40] T. Kubo, A. Nakahira, J. Phys. Chem. C 112 (2008) 1658–1662.
[41] A. Nakahira, W. Kato, M. Tamai, T. Isshiki, K. Nishio, H. Aritani, J. Mater. Sci. 39 (2004) 4239–4245.
[42] J. Hu, J. Deng, S. He, Z. Chang, J. Zhao, J. Liu, Mater. Sci. Eng. 19 (2001) 71–74.
[43] T. Kawahara, Y. Konishi, H. Tada, N. Tohge, J. Nishii, S. Ito, Angew. Chem. Int. Ed. 41 (2002) 2811–2813.
[44] H. Tada, M. Tanaka, Langmuir 13 (1997) 360–364.
[45] Z. Ding, G.Q. Lu, P.F. Greenfield, J. Phys. Chem. B 104 (2000) 4815–4820.
[46] K. Tanaka, M.F.V. Capule, T. Hisanaga, Chem. Phys. Lett. 187 (1991) 73–76.
[47] A. Thorne, A. Kruth, D. Tunstall, J.T.S. Irvine, W.Z. Zhou, J. Phys. Chem. B 109 (2005) 5439–5444.
[48] S.Q. Song, P. Tsiakaras, Appl. Catal. B-Environ. 63 (2006) 187–193.
[49] D.V. Bavykin, F.C. Walsh, J. Phys. Chem. C 111 (2007) 14644–14651.
[50] J.W. Long, R.M. Stroud, K.E. Swider-Lyons, D.R. Rolison, J. Phys. Chem. B 104 (2000) 9772–9776.
[51] D.R. Rolison, P.L. Hagans, K.E. Swider, J.W. Long, Langmuir 15 (1999) 774–779.
[52] R. Manoharan, J.B. Goodenough, J. Mater. Chem. 2 (1992) 875–887.
[53] Z.L. Liu, X.Y. Ling, X.D. Su, J.Y. Lee, J. Phys. Chem. B 108 (2004) 8234–8240.
[54] H. Razmi, E. Habibi, H. Heidari, Electrochim. Acta 53 (2008) 8178–8185.
[55] V. Rao, Hariyanto, C. Cremers, U. Stimming, Fuel Cells 7 (2007) 417–423.
[56] N. Fujiwara, K.A. Friedrich, U. Stimming, J. Electroanal. Chem. 472 (1999) 120–125.